Chemical and Process Engineering: New Frontiers
DOI: 10.24425/cpe.2024.149464

Dynamics of the phenomenon of immiscible viscous fingering in porous media - experimental studies and model description

Mariola Błaszczyk[1]*, Magdalena Wróbel-Jędrzejewska[2], Łukasz Przybysz[1,2], Aleksandra Budzyń[1]

[1]Lodz University of Technology, Faculty of Process and Environmental Engineering, Department of Chemical Engineering, Address: 213 Wolczanska St., 90-924 Lodz, Poland

[2]Prof. Wacław Dąbrowski Institute of Agriculture and Food Biotechnology - State Research Institute, Department of Technology and Refrigeration Techniques in Lodz, Al. Marszałka J. Piłsudskiego 84, 92-202 Lodz, Poland

*corresponding author, e-mail: mariola.blaszczyk@p.lodz.pl

Mariola Błaszczyk ORCID: 0000-0001-6397-568X
Magdalena Wróbel – Jędrzejewska ORCID: 0000-0002-7633-5398
Łukasz Przybysz ORCID: 0000-0003-3581-9414

Abstract

Improvement of life quality, food production and sustainability requires search for better, efficient natural resources extracting methods, while minimizing environmental impact, which is determined by carbon and water footprint calculation. In order to counter global phenomena, it is necessary for food-producing chain to work together to take conscious action on environment. Restoring balance demands action to reduce greenhouse gas emissions and rational water use, by reducing energy intensive processes or increasing efficiency of wastewater treatment methods. This requires a thorough understanding of all phenomena that determine a given process. Viscous fingering occurs during such processes as enhanced oil recovery, metal crystallization in batteries, sugar refining, groundwater purification and many others. Research to improve knowledge of this phenomenon and ability to predict its effects is crucial in development of basic industrial processes. This paper presents an experimental

This article has been accepted for publication and undergone full peer review but has not been through the copyediting, typesetting, pagination and proofreading process which may lead to differences between this version and the version of record. Please cite this article as DOI: 10.24425/cpe.2024.149464.

Received: 25 March 2024 | Revised: 05 July 2024 | Accepted: 23 August 2024

study of tracking immiscible viscous fingering in modified Hele-Shaw cells filled with a granular bed of known parameters. The influence of bed parameters and flow conditions on the observed phenomenon was investigated. During the tests, beds with the following grain diameter ranges were used: 200–300, 300–400 and 400–600 μm; the liquid was injected at three different flow rates in the range of 100–400 ml/h. On the basis of carried out work, a model of the studied phenomenon was proposed, which made it possible to determine the extent and the fingering scale.

Keywords: viscous fingering; porous media; fluid displacing; carbon footprint; water footprint; economic benefits

1. Introduction

The main goal of mankind is to ensure a decent existence for everyone. A key role is therefore played by the rapidly growing global economy, which unfortunately causes shrinkage of natural resources and progressive degradation of the environment at every stage of production. In order to pursue sustainable development, it is necessary to search for new, more efficient, and optimize existing industrial processes also in the agro-food production. Food production is one of the areas of human activity contributing to the excessive consumption of natural resources and energy (Law et al., 2020). In order to counteract global trends, it is necessary for the entire chain of food-producing entities to work together on an ongoing basis and to take environmentally conscious measures. Agriculture and the agro-food industry contribute significantly to greenhouse gas (GHG) emissions and water consumption (Lahtinen et al., 2022; Mazis et al., 2021; Pałaszyńska and Juszczak, 2018). Climate change, global warming, water and energy shortages are internationally recognized as problems that require immediate action. Restoring ecological balance demands urgent action to reduce GHG emissions and rational water use, i.e. minimizing carbon footprint (CF) and water footprint (WF). By getting to know which activities cause the greatest emissions or water demand, it is possible to influence their reduction more precisely, primarily by introducing more economical solutions (Liobikienė and Rimkuvienė, 2020). Identifying these areas and providing directions for their reduction is a complex issue. Any action must be targeted so as not to threaten food security. One method of minimizing CF is to reduce energy intensity of processes, while for WF is to use effective methods of treating wastewater from industry, especially the agro-food sector (Yousefi et al., 2017). For this purpose, it is necessary to understand all the phenomena occurring during a given process, which can have a positive or

negative impact on its course. Some of the more interesting issues are the phenomena occurring during multiphase fluid flows in porous media. When a low-viscosity fluid displaces a high-viscosity fluid, interfacial instabilities occur, which can lead to a phenomenon commonly referred to as viscous fingering (VF). This interfacial instability occurs during many industrial processes, such as in sugar refining, oil recovery, hydrology, filtration and tissue engineering. The phenomenon of fingering, can be used to increase the efficiency of industrial processes where intensive mass or heat exchange is required. By increasing the contact area between phases, the fingering can speed up chemical reactions and heat exchange, which can lead to reduced energy and material consumption. In addition, the fingering can be used in phase separation processes such as distillation, which also leads to energy and water savings and increased process efficiency. The VF phenomenon can also be undesirable in many cases, for example, the formation of dendrites reduces battery life (Arguello et al., 2022). When conducting methods to enhance oil recovery by injecting liquid or gas into the reservoir, the fingering phenomenon reduces productivity (Yang et al., 2022; Zhang et al., 2011a). Whatever impact this phenomenon has on a process, understanding its nature and being able to predict its effects is of great importance, so research in this area can contribute to improving the efficiency and productivity of various industrial processes, as well as developing new, less energy-intensive and less-consuming components, technologies and production methods. Experimental studies of VF phenomena are carried out using so-called Hele-Shaw cells (HSC) or directly in a porous medium. The study of VF patterns observed in Hele-Shaw cells is used to describe the phenomena in the formation of snow crystals, the formation of dendrites in the case of metal crystallization, metal deposition in the case of electrolytic process and the spread of bacterial colonies, etc. (Pinilla et al., 2021; Singh et al., 2020). A Hele-Shaw cell (HSC) is a device in which two transparent parallel glass plates are separated by a very small gap. The VF phenomenon in the case of a vertical HSC is driven by the combined effect of viscous force and gravitational force (density). But in the case of horizontal HSC, the interfacial instability is driven only by the viscous force. Existing studies have typically been limited to tracking the extent of the phenomenon (Jamaloei, 2021).

The viscous fingering phenomenon can be divided into two types. The first, called Immiscible Viscous Fingering, is characterized by the presence of an interface, and the main driving force, causing finger patterns at the front of fluid displacement, is the viscosity gradient caused by the difference in viscosity of the phases. The second type is Miscible Viscous Fingering, in which there is no clear interface between the moving phases, there are

strong diffusion effects caused by changes in concentration (Jha et al., 2011; Malhotra et al., 2015).

Numerous theoretical works have been carried out to develop mathematical models capable of describing the dynamics of both types of displacements. For example, works (Pinilla et al., 2021; Singh et al., 2020) have summarized the leading theory on both types of displacements, starting with Hele-Shaw flow and ending with approaches describing flow through porous media. There are also experimental papers in the literature on various aspects of this phenomenon, In the case of tracking VF in porous media, it is particularly problematic in terms of measurement techniques. The image processing technique proposed by Peters et al. (1987) involved using cross-sections of porous bed cores to visualize finger lengths, areas and pattern frequencies. Despite its innovation, the technique was slow and inefficient because it required the destruction of core samples, where the author recommended a non-intrusive or non-destructive approach (Pinilla et al., 2021). It is more common to create various types of micromodels for research purposes. In the literature, one can find many works (Doorwar and Mohanty, 2015; Doorwar and Mohanty, 2017; Jamaloei et al., 2016; Jamaloei 2021; Zhang et al., 2011b), where pore network properties were mapped using more or less complex physical models. However, the results of studies based on these measurements are often difficult to relate to the actual conditions in the deposits, so their application is limited. The tracking of the phenomenon of Immisible Viscous Fingering, was also carried out using Hele-Shaw cell (Li et al., 2009; Sinha and Tarafdar, 2009). The advantage of this method is the simplicity and ease of reproducing the experiment under different conditions. However, most often the tests are conducted at zero or low porosity, which means that in order to relate the results of these tests to real flows in porous media, calculations based on various types of simulations are necessary. In this work, it was decided to overcome this limitation, and a Hele-Shaw cell design was used for the study, in which a high-viscosity liquid saturated granular bed with known parameters. A lower viscosity liquid was injected into such a cell and VF tracking was performed.

Based on the work present in the literature on VF phenomena using HSC, the researchers found that the main active control parameters of VF anomalies are - injection rate Q [ml/h], the distance between the plates or the thickness of the fluid layer, the viscosity ratio of the fluids and their surface tension (Singh et al., 2020). These parameters have been considered to determine the formation of specific patterns during the VF process. However, there is a lack of experimental work that takes into account the influence of parameters also of the porous medium on this phenomenon, such as porosity, permeability and also the saturation

of the bed with the eluted fluid. There are many works in the literature devoted to modeling the fingering phenomenon (Belotserkovskaya and Konyukhov, 2010; Kampitsis et al., 2020; Lagree et al., 2016; Li and Riviere, 2016; Mostaghimi et al., 2016; Wang et al., 2019). The results of these works allow the formation of various types of simulations that would be able to more or less accurately predict the way fingering spreads under specific conditions. However, many of these numerical models are based on hypothetical assumptions, while their reference to specific cases requires going through a time-consuming and often complicated computational procedure. Therefore, the practical use of these works is limited. Simpler models that take into account both fluid and bed parameters and consider given flow conditions are needed to determine how fast and in which way the VF phenomenon will occur.

For this reason, in the present study, an attempt is made to model the fingering process based on the experimental data obtained, using a modified Blake-Kozeny-Caman theory (Carman, 1937) originally used to describe single-phase transport in porous media. This will make it possible to estimate in a simple way the extent of the fingering phenomenon under the given conditions and how widespread it will be. This will allow, through the use of scaling methods, to quantitatively predict how much impact the VF phenomenon has on a particular industrial process. This could be useful for determining the reduction in oil recovery when conducting specific recovery methods, or predicting how quickly metallic dendrites will form in lithium-ion batteries. These issues are a huge challenge of today's times, and the development of knowledge in this area can contribute to a more efficient and sustainable use of natural resources and minimize the environmental impact of industry (Ledakowicz and Ziemińska-Stolarska, 2023), especially in the agro-food sector.

2. Experimental methodology

The study of the fingering phenomenon was carried out using a dedicated test stand, the diagram of which is shown in Fig.1

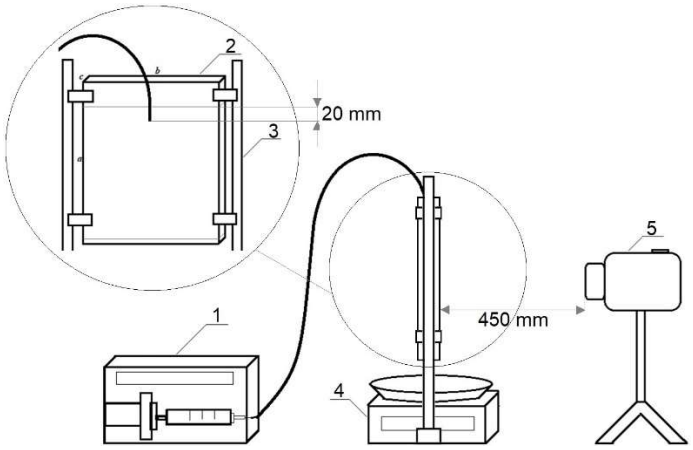

Figure 1. Schematic of the test stand: 1 - syringe pump, 2 - measuring container, 3 - stand, 4 - vessel with balance, 5 - digital camera.

The test stand consisted of a container made of transparent plastic (Plexiglass) in the shape of a cuboid with dimensions vertical: 26.5 cm, horizontal: 11.5 cm and thickness: 1.5 cm. The container was mounted vertically on racks with handles, the upper part was left open, while a metal mesh was mounted on the lower part to protect the deposit from falling out. A silicone hose with an inner diameter of D = 5 mm was mounted to the container, through which the washing liquid (water) was fed. This liquid was pumped under a preset flow rate using a syringe pump. The container was completely filled with the test medium, which was a mixture of glass microspheres of different grain size fractions and EMULGOL ES 12 oil (viscosity 0.062 Pa·s, density 880 kg/m^3, surface tension 26+/- 1.3 mN/m) from the manufacturer PKN ORLEN.

Glass microspheres produced by Alumetal-Technik were used. The material was characterized by a smooth surface, round shape and chemical inertness. The density was 2.5 g/cm^3. The chemical composition of the microspheres was as follows: 70-73% - SiO_2, 13-15% - $Na_2O + K_2O$, 7-11% - CaO, 3-5%- MgO, 0.5-2.0% - Al_2O_3 and $TiO_2 \leq 0.1\%$. Microspheres of 3 different grain size fractions were used in this study, with the range of diameters shown in Table 1.

Table 1. The parameters of the glass microspheres used in the study and the amounts of oil saturation.

Symbol	Grain size fraction [μm]	Average grain size, d_{zr} [μm]	Porosity [-]
Z1	400–600	500	0.36
Z2	300–400	350	0.34
Z3	200–300	250	0.34

The refractive indexes of all used media are as follows: Plexiglass (1.49); Glass (1.50); Distilled water (1.34); EMULGOL ES 12 (1.44).

The mixture of microspheres with oil was made in such proportions as to obtain a total oil saturation degree of the bed S_n = 1 [-] (where S_n is defined as the ratio of the volume of space occupied by the substance to the volume of void spaces in the bed). The volume of void spaces indicates the porosity of the bed. The procedure for saturating the bed with oil was to first pour the dry bed into a test container, then transfer it to a measuring cylinder. Knowing the volume of the bed in the container and the porosity of the bed, it was possible to determine the volume of oil needed to achieve complete saturation. The measured amount of oil was mixed thoroughly with the bed and then placed back into the test container, making sure that the bed was evenly distributed throughout the container. Then the process of pumping the washing liquid, which was distilled water (viscosity 0.0011 Pa·s, density 998 kg/m^3, surface tension 72+/-1.7 mN/m), into the bed began. After setting the flow rate, the washing liquid flowed into the bed. The mixture of the washing liquid and oil underwent immediate self-emulsification, so that the color of the liquid turned white. This made it possible to visually track the fingering process. The process was recorded with a camera Sony HDR-CX405 [effective pixel count: approx. 2.29 megapixels (16:9), approx. 1.71 megapixels (4:3); focal length: f = 26.8–804.0 mm (16:9), f = 32.8–984.0 mm (4:3); photo size: 9.2 megapixels, 16:9 (4032×2272 px) 6, 2.1 megapixels, 16:9 (1920×1080 px)]. The experiments were carried out in daylight, and no additional light source was used. Tests were conducted for individual deposits at three preset flow rates: 400 ml/h, 200 ml/h and 100 ml/h. The total amount of washing liquid was 60 ml. Each test was repeated three times, and the obtained results were averaged. The process of penetration of the oily bed with the washing liquid was carried out until a stream of washing liquid ran through the entire length of the bed or until the washing liquid was exhausted (60 ml).

The obtained films were analyzed using SigmaScanPro 5 and LevenhukLite software. This made it possible to determine the changes over time of the total area undergoing the fingering process. In addition, changes over time in the extent of the process after an angle from 0 to 180^o were determined.

The CAS numbers of the chemicals used are as follows: EMULGOL ES 12 (64742-52-5), glass microspheres (69012-64-2), distilled water (7732-18-5).

3. Analysis of results

From the study, films were obtained that, when processed, made it possible to follow the fingering process over time. Fig. 2 shows example photos of the process, in which it is possible to observe how streams of washing liquid make their way through the oily bed. These photos refer to the process captured 240s after the start of the liquid feed at an inflow rate of 400 ml/h. The bed through which the liquid moved had grain size in the range of 400 to 600 μm.

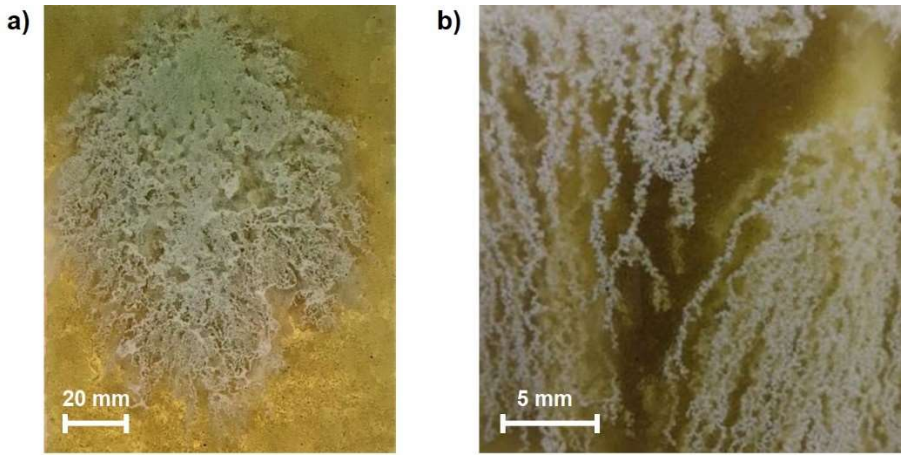

Figure 2. Example images of the fingering process (Z1 bed, Q_v=400 ml/h, t = 240s); a) overall view, b) magnification view.

As can be observed in the photo (Fig. 2a), the farther away from the point of delivery of the washing liquid, the more clearly the individual streams can be seen, which form more or less spread out trees. In the magnified photo (Fig. 2b), it can be observed that the streams can branch, intertwine and weld together repeatedly to form a complex network. The development over time of this type of tree has been modeled many times in various works on the subject in the literature (Belotserkovskaya and Konyukhov, 2010; Kampitsis et al., 2020; Lagree et al., 2016; Li and Riviere, 2016; Mostaghimi et al., 2016; Wang et al., 2019). However, these models were mostly based on theoretical grounds, these experiments can provide a basis for their experimental verification.

The distribution and extent of the resulting trees depends on both the intensity of the washing liquid inflow and the grain size fraction of the bed. In order to compare these parameters with each other, Fig. 3 presents a summary of photos of the fingering process taken (a) for different inflow intensities of washing liquid Q_v [ml/h] and (b) for different grain size fractions of the bed as a function of time. The actual dimensions of each photo are 26×11 cm.

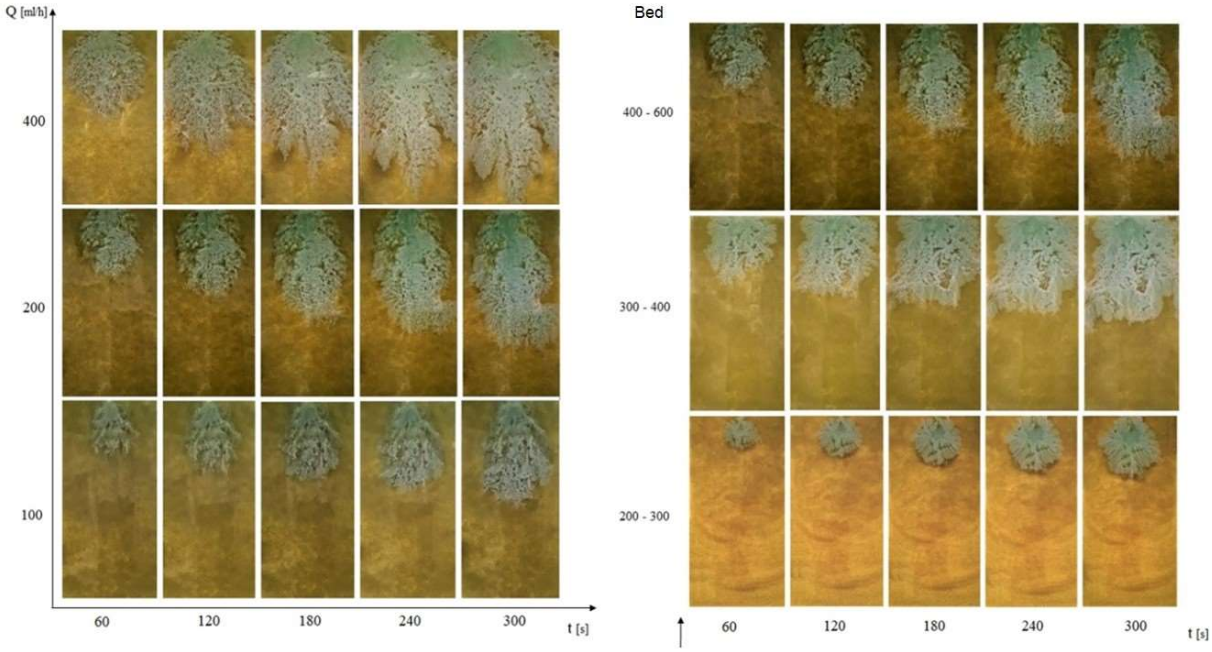

Figure 3. Summary of images of the fingering process (a) for different inflow intensities of washing liquid Q_v [ml/h] as a function of time for 400–600 μm bed; (b) for different bed grain size fractions as a function of time at an inflow rate of 400ml/h.

As can be observed from the images captured over time, the growth of the trees is more intense the higher the intensity of the inflow of washing liquid, but the differences are more noticeable after a longer time (200–300s). The trees become larger, but their formation looks similar at any given Q_v [ml/h] (as was observed during the experiment). Differences in the shape of the trees can be observed by considering a comparison of the process taking place in different fractions of deposits (Fig.3.2b). In a deposit where the grains are in the range of 200–300 μm, the trees take on a different shape and size than in deposits with a larger grain size fraction. First of all, the trees form compact areas, and are not spread out even after a longer period of time. With such compact deposits, the liquid meets great resistance to penetrate the structure, so the range of fingering is not large. In the case of deposits with larger grain size fractions, it is already clear that the trees are highly branched, and the range of individual paths is many times longer. Thus, on the basis of visual analysis alone, it can be concluded that the gradation of the deposit has a huge impact on the intensity of the process and the way oil is washed out of the oily deposit. However, visual analysis alone does not provide measurable results, so the recorded videos were analyzed in terms of the spread of the trees and their extent. Based on the analysis of the images, it was possible to measure the change in the area of the bed occupied by the eluting fluid A_z [m^2] over time,

258 which, when divided by the total area of the bed A_c [m^2], gave a parameter called here the
259 spreading factor ε_w [-], calculated from the relationship:

260 $$\varepsilon_w = \frac{A_z}{A_c} \quad (1)$$

261 The spreading factor represents the ratio of the volume of the space through which the flow
262 takes place to the entire bed, but for HSC cells it is calculated as a ratio of surface area (the
263 third dimension - depth - was neglected).
264 Fig. 4 presents a plot of the time dependence of spreading factor ε_w at different liquid inflow
265 rates Q_v for different grain size fractions of the bed.

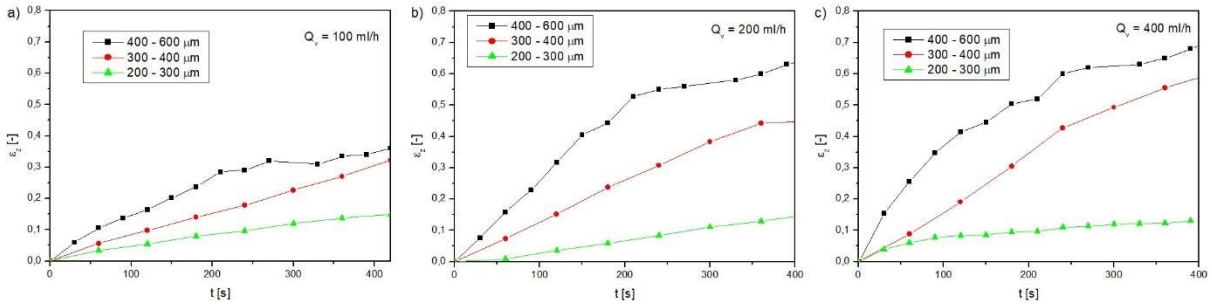

266

267 Figure 4. Changes of spreading factor over time for different grain size fractions of the bed (a)
268 Q_v = 100 ml/h, (b) Q_v = 200 ml/h, (c) Q_v = 400 ml/h.

269 As can be observed from the graphs of the dependence of the coefficient ε_w on time in
270 the initial stage of the process, this parameter increases cubically, but after some time the
271 increase is smoother. The grain size of the deposit is of great importance for the process. For
272 deposits with a larger grain size fraction, the degree of spreading is much greater than for
273 deposits with smaller average grain diameters at the same inflow rates of the washing liquid
274 after the same time elapses. For example, for the deposit with the smallest grain size fraction
275 (200–300 µm) after 420 s, the spreading parameter was more than double lower than that of
276 the process with the largest grain size fraction (400–600 µm) at an inflow rate of Q_v = 100
277 ml/h, and more than 4.5-times lower at an inflow rate of Q_v = 400 ml/h.

278 Interestingly, the liquid inflow rate does not affect the ε_w [-] parameter as much,
279 especially for deposits with small grain diameters. In a bed with a grain size fraction of 200–
280 300 µm, a spreading parameter of 0.13–0.15 after 420s was observed regardless of the flow
281 rate. In the case of a 300–400 µm bed, the differences are already much greater, as at Q_v = 100
282 ml/h in the same time the spreading parameter was 0.32 and at twice the Q_v the parameter ε_w
283 increased by a third of its value. A fourfold increase in the inflow rate, on the other hand,
284 resulted in a nearly twofold increase in the spreading parameter for this bed. In the case of the

bed with the largest grain size fraction (400–600 μm), large differences in the ε_w coefficient could be observed between an inflow rate of 100 ml/h and twice as much because here an almost twofold increase in this parameter was observed, while an increase in the flow rate to 400 ml/h no longer caused large changes in the spreading parameter.

In addition to the surface area of the elution liquid itself, the shape of the tree that forms during the elution process is also important. Whether the branches spread sideways or rather point vertically downward can determine what the efficiency of oil recovery from a given deposit will be. In order to show how the shape of the spreads changed in each deposit, an analysis of the resulting images was carried out taking into account the distance (range) of the tree arm in a given direction. This distance was measured from the point of introduction of the washing liquid. This distance was measured at an angle starting from the horizontal (0° angle) in 30° increments up to an angle of 180°. Thus, an angle of 90° meant the vertical direction down directly below the liquid insertion point. The method of measurement is shown schematically in Fig. 5.

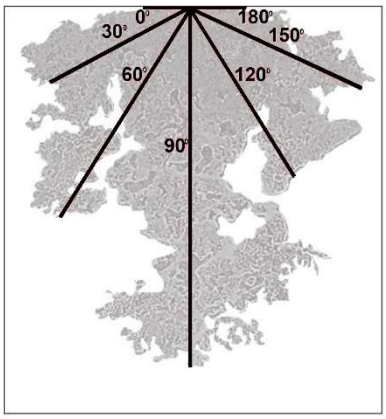

Figure 5. Schematic for marking the evolution range of a tree.

As a result of measuring the distance from the spreading point L after the angle α [°], it was possible to plot the dependence of $L(\alpha)$ after time for different fractions of deposits where the process took place at different inflow rates Q_v. This resulted in nine graphs, which are posted collectively in Fig. 6. The standard deviation at each measurement did not exceed 6%.

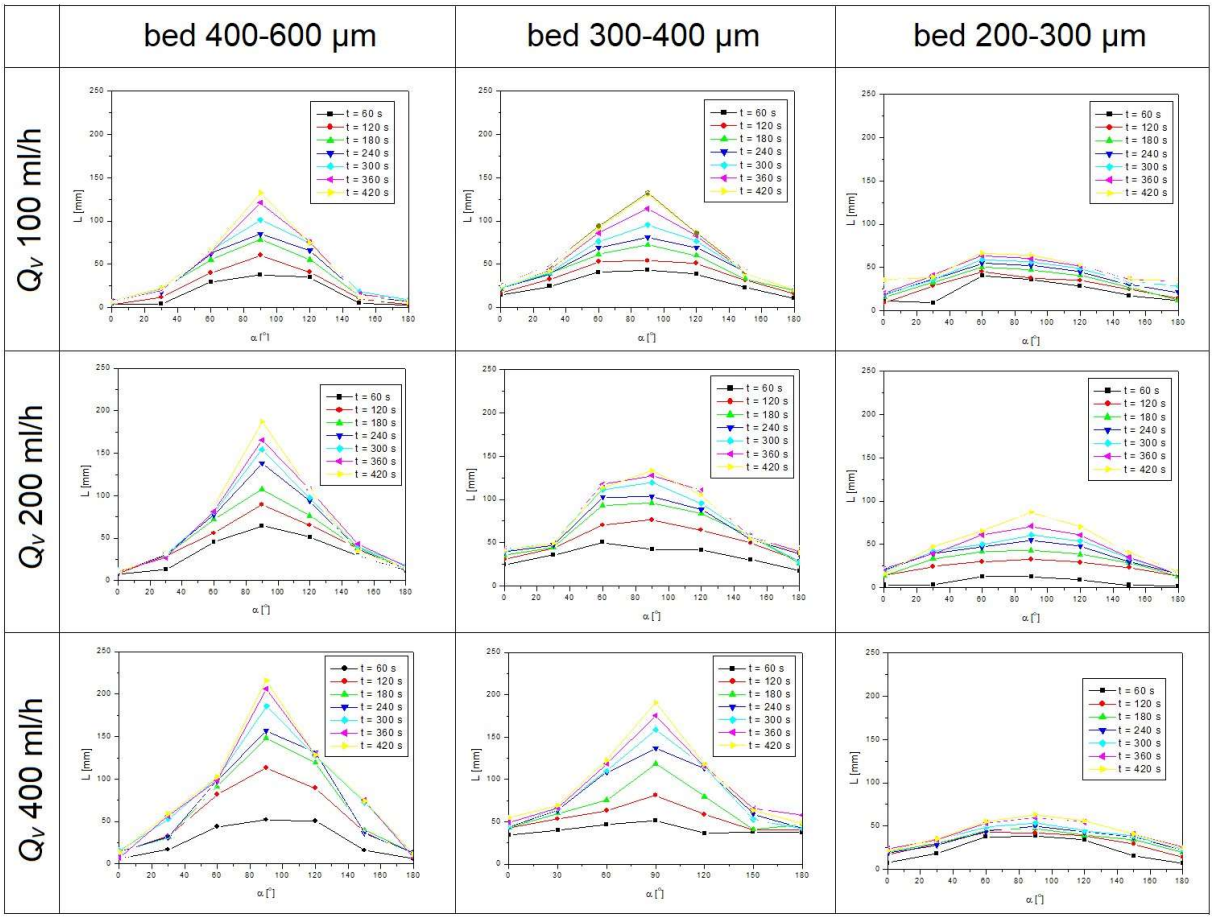

Figure 6. Change in the extent of the tree relative to the angle during the washout process.

Based on the graphs in Fig. 6, it is possible to follow how the shape of the spill (tree) changed during the process of injecting the washing liquid. Introducing the resulting graphs against bed fraction and inflow rate allowed comparing how these parameters affected the spread of the resulting trees. It can be observed that the largest ranges of $L(\alpha)$ were found in the bed with the largest grain size fraction. With the passage of time, the range of L [m] at the 90° angle was clearly larger than the ranges at other angles, indicating that the main direction of transport was vertical. Since the deposit was not strongly compact, there was also no high flow resistance, which meant that the fluid could flow downward by gravity, without having to seek more accessible paths in other directions. In the case of this deposit, the inflow rate of the washing liquid played a greater role on the L reach than in the case of deposits with smaller average grain size. Comparing the range of L after a 90° angle at a time of 420s, recorded at an intensity of 100 ml/h, with twice the intensity, an increase of more than 44% can be observed, while with four times the inflow intensity, the increase is 54%. For deposits with smaller grain size fractions, the extents of L after all directions are also smaller. For a

200–300 μm deposit, the maximum range at 90° after a time of 420s was almost 2.5 times smaller than for a 400–600 μm deposit at the same flow rate. In the case of the bed with the smallest average grain diameter, small differences between the *L*-ranges at different angles can also be observed. This means that with such compact beds, the flow resistance was high enough so that the fluid could not flow directly by gravity downward, but sought other flow paths, including in other directions. For this reason, the shape of the trees in these beds is more circular (see Fig. 3b). The intensity of fluid inflow for these deposits plays a lesser role than for less compact deposits, since the extents of L at different Q_v are not drastically different from each other.

4. Process modeling

The experimental studies carried out have made it possible to quantitatively measure how the shape, extent and area of the resulting washing liquid trees depend on the degree of grain size of the bed and on the inflow rate of the washing liquid. However, in order for this knowledge to be useful, it is necessary to make generalizations so that reference can be made to any bed at any scale. To do this, the Blake-Kozeny-Caman theory was used (Carman, 1937; Paidoussis, 1998). According to this theory, a granular deposit can be treated as a bundle of tortuous capillaries. The value of the pressure drop Δp [Pa] in such a granular bed, through which the fluid flows, can be expressed by the relation:

$$\Delta p = f_{BK} \frac{L_z}{d_{zr}} \frac{1-\varepsilon}{\varepsilon^3} v_0^2 \rho \tag{2}$$

where: L_z – bed length [m], ε – porosity [-], d_{zr} – average grain diameter of the bed [m], v_0 – liquid flow rate [m/s], ρ – emulsion density [kg/m^3].

The parameter f_{BK} [-] is a coefficient of friction that can be determined using the formula:

$$f_{BK} = \frac{A_{BK}}{Re_{BK}} \tag{3}$$

where: A_{BK} – constant [-], a Re_{BK} – modified form of Reynolds number [-]:

$$Re_{BK} = \frac{v_0 d_{zr} \rho}{\eta(1-\varepsilon)} \tag{4}$$

where: η – emulsion viscosity [Pa·s].

For the purposes of the study, a distribution factor F_M [-] was introduced instead of f_{BK} [-] (in Relation 2). This modification consists in introducing the spreading factor ε_w [-] defined by Equation (1) instead of the bed porosity ε [-], After making this assumption and transforming Equation (2), the F_M [-] factor can be written as:

$$F_M = \frac{\Delta p}{v^2} \frac{d_{zr}}{L_z \rho} \frac{\varepsilon_w^3}{1-\varepsilon_w} \tag{5}$$

where: v – velocity of liquid flow in capillaries [m/s], ε_w – spreading factor [-] (Equation (1)), F_M - distribution factor [-], Δp is calculated based on the Hagen - Poiseuille relationship:

$$\Delta p = \frac{128\, Q_v\, \eta\, L_{90}}{\pi D^4} \tag{6}$$

where: Q_v – washing liquid inflow rate, L_{90} – the range of the tree after the 90º angle [m] (see Fig. 5), D – diameter of washing liquid inlet [m].

Velocity of the wash liquid was calculated as:

$$v_w = \frac{L_{90} \cdot K_r}{t_c} \tag{7}$$

where: K_r is the tortuosity of the channels, taken as the value of 1.41 [-] (Dullien 1992), t_c – final measuring time [s].

The velocity value v was calculated as the average of the discharge velocity from the dispensing tube and the velocity determined by Equation (7). While the spread number R_M [-] defined for the process under consideration was:

$$R_M = \frac{C\, v d_{zr} \rho}{\eta(1-\varepsilon_w)} \tag{8}$$

where: C – parameter dependent on the bed and flow rate [-].

The constant C was determined empirically, its values are presented in Table 2.

Table 2. Summary of parameter C.

	Q_v 400 ml/h	Q_v 200 ml/h	Q_v 100 ml/h
bed 400–600 µm	0.9	1.1	3.5
bed 300–400 µm	2.8	3.1	6.8
bed 200–300 µm	2.1	3.3	7.3

Knowing all the bed and fluid parameters and using the measured values of ε_w and L_{90} over time for all the tests performed, it was possible to calculate the F_M values using Equations (5) and (6) and (7) and the corresponding R_M values using Equation (8). With the appropriate choice of the constant C (Table 2), it was possible to obtain the dependence of F_M on R_M for all measurements, which is presented in the graph of Fig. 7. In the calculations the density ρ and viscosity η were taken as the density and viscosity of the washing emulsion, equal to 978 kg/m^3 and 0.0021 Pa·s, respectively.

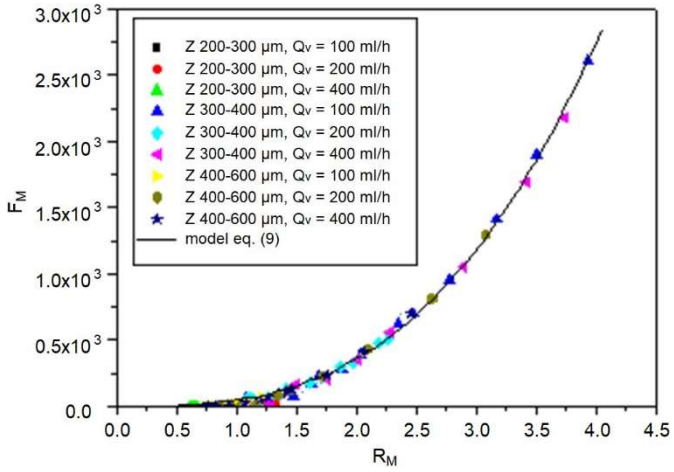

Figure 7. Dependence of F_M factor on spread number R_M.

As can be observed in Fig. 7, the experimental points of the dependence of the F_M factor on the spread number R_M for all data are arranged with respect to a power curve. Therefore, the data were described by the following equation:

$$F_M = AR_M^B \tag{9}$$

where: *A, B* – parameters of this equation equal to 46.97 and 2.934 [-], respectively, and determined using Origin 6.0 software. The accuracy of the fitting is equal to R^2=0.986.

The previous considerations can be used to determine the spreading factor parameter ε_w, Equation (5) can be transformed to the form where the unknown is ε_w, then a third degree equation is obtained:

$$\frac{\Delta p}{F_M {v_0}^2 \rho}\frac{d_{zr}}{L_z}{\varepsilon_w}^3 + \varepsilon_w - 1 = 0 \tag{10}$$

Equation (9) can be substituted as the F_M factor, while the R_M number can be described by Eq. (8), then a relationship is obtained:

$$\frac{\Delta p}{A\left[\frac{C\, v_o d_{zr}\rho}{\eta(1-\varepsilon_w)}\right]^B {v_0}^2 \rho}\frac{d_{zr}}{L_z}{\varepsilon_w}^3 + \varepsilon_w - 1 = 0 \tag{11}$$

As a result of such transformations, a polynomial was obtained, which, using available calculation programs (MathCad, Mathlab, etc.), makes it possible to calculate the root of the equation. Thus, knowing the parameters of the bed (d_{zr}, L_z), and the parameters of the fluid (η, ρ), having data at what speed the fluid flows v_0 and how its range in the vertical direction (L_{90}) changes, it is possible to estimate the spreading factor ε_w for specific process conditions. Of course, in order to use this approach, it is necessary to know the constants *A, B* and *C*, which

401 can be obtained by conducting a limited number of laboratory-scale experiments. With these
402 data available, it will be possible to estimate the results for any scale.
403
404 **5. Summary and conclusions**
405 This paper presents the results of viscous fingering phenomenon carried out in a
406 modified Hele-Shaw cell, in which granular beds with different parameters were placed.
407 These beds were saturated with a high-viscous liquid (oil), the value of the degree of
408 saturation was 1. A low-viscous liquid (water) was injected into the cell under a preset inflow
409 rate, which formed characteristic flow paths in the form of trees in the oily bed. The shape,
410 growth and character of these trees were studied depending on the parameters of the bed as
411 well as on the flow conditions. As a result, a quantitative description of the phenomenon was
412 obtained. A spreading factor parameter was introduced, allowing comparison of the spreading
413 trees over time.
414 A mathematical description of the process was proposed using the Blake-Kozeny-Carman
415 theory, which was originally developed for single-phase flows through porous media. The
416 theory is based on the concept of a capillary bundle through which fluid flow takes place.
417 With this theory, it is possible to determine the diameter, curvature and number of capillaries
418 based on the knowledge of the parameters of the granular bed. By introducing a spreading
419 factor relating to the fingering phenomenon instead of the porosity of the bed, with the
420 knowledge of changes in the extent of the spreading of the trees over time, it was possible to
421 determine a modified resistance coefficient. By comparing the values of these coefficients
422 with the corresponding values of the spread number R_M, it was possible to obtain a
423 relationship described by a power curve. Knowing the parameters of this curve, determined on
424 the basis of experimental data, it is possible to obtain a relationship that allows to determine
425 the spreading factor for any scale of the process. The proposed modeling approach can
426 provide an alternative to time-consuming and often complicated methods based on numerical
427 simulations for predicting the fingering phenomenon in porous media. This may influence the
428 development of new, less energy and ingredient consuming methods of wastewater treatment
429 used in the industry especially in agriculture sector, minimizing the carbon and water
430 footprint of food products. This will transform into environmentally friendly activities in line
431 with sustainable development trends, which is the direction of progress in every field of
432 industry supported by international strategies.
433
434

ACKNOWLEDGEMENT

This research was funded by National Science Center (Kraków, Poland), grant number Sonata 2019/35/D/ST8/01033.

REFERENCES

Arguello M.E., Labanda N.A., Calo V.M., Gumulya M., Utikar R., Derksen J., 2022. Dendrite formation in rechargeable lithium-metal batteries: Phase-field modeling using open-source finite element library. *J. Energy Stor.,* 53, 104892. DOI:10.1016/j.est.2022.104892

Belotserkovskaya M., Konyukhov A., 2010. Numerical simulation of viscous fingering in porous media. *Phys. Script*., 142, 014056.

Carman P.C., 1937. Fluid Flow through granular beds. *Trans IChemE*., 15, 150–166.

Doorwar S., Mohanty K.K., 2015. Fingering function for unstable immiscible flows. *SPE Reservoir Simulation Symposium*, Houston, Texas, USA.

Doorwar S., Mohanty K.K., 2017. Viscous-fingering function for unstable immiscible flows (includes associated erratum). *SPE J*. 22, 1, 19–31.

Dullien F.A.L., 1992. *Porous Media Fluid Transport and Pore Structure*. California: Acad. Press Inc.

Jamaloei B.Y., Babolmorad R., Kharrat R,. 2016. Visualization and analysis of viscous fingering in alcohol-assisted surfactant waterflooding of heavy oil in a two-dimensional sandstone micromodel. *Fuel*, 184, 169–179.

Jamaloei B.Y., 2021. Effect of wettability on immiscible viscous fingering: Part I. Mechanisms. *Fuel,* 304, 120726. DOI:10.1016/j.fuel.2021.120726

Jha B., Cueto-Felgueroso L., Juanes R., 2011. Fluid mixing from viscous fingering. *Phys. Rev. Lett*. 106, 19, 194502. DOI:10.1103/PhysRevLett.106.194502

Kampitsis A.E., Adam A., Salina P., Pain C.C., Muggeridge A.H., Jackson M.D., 2020. Dynamic adaptive mesh optimisation for immiscible viscous fingering. *Comput. Geosci*. 24, 3, 1221–1237.

Lagree B., Zaleski S., Bondino I., 2016. Simulation of viscous fingering in rectangular porous media with lateral injection and two- and three-phase flows. *Transp. Por. Media,* 113, 3, 491–510.

Lahtinen L., Mattila T., Myllyviita T., Seppälä J., Vasander H., 2022. Effects of paludiculture products on reducing greenhouse gas emissions from agricultural peatlands. *Eco. Eng*. 175, 106502. DOI:10.1016/j.ecoleng.2021.106502.

Law E.P., Arnow E., Diemont S.A.W., 2020. Ecosystem services from old-fields: Effects of site preparation and harvesting on restoration and productivity of traditional food plants. *Eco. Eng*. 158, 105999. DOI:10.1016/j.ecoleng.2020.105999.

Ledakowicz S., Ziemińska-Stolarska A., 2023. The role of life cycle assessment in the implementation of 1 circular economy in sustainable future. *Chem. Proc. Eng. New Front.,* 44, 4. DOI: 10.24425/cpe.2023.147396

Li S., Lowengrub J.S., Fontana J., Palffy-Muhoray P., 2009. Control of viscous fingering patterns in a radial hele-shaw cell. *Phys. Rev. Lett*. 102, 17. DOI:10.1103/PhysRevLett.102.174501

Li J., Riviere B., 2016. Numerical modeling of miscible viscous fingering instabilities by high-order methods. *Transp. Por. Media,* 113, 3, 607–628.

Liobikienė G., Rimkuvienė D., 2020. The role of income inequality on consumption-based greenhouse gas emissions under different stages of economic development. *Environ. Sci. Pollut. Res*. 27, 43067–43076. DOI:10.1007/s11356-020-10244-x

Malhotra S., Sharma M.M., Lehman E.R., 2015. Experimental study of the growth of mixing zone in miscible viscous fingering. *Phys. Fluids*, 27, 1, 014105. DOI:10.1063/1.4905581

Mazis A., Litskas V.D., Platis D.P., Menexes G.C., Anagnostopoulos C.D., Tsaboula A.D., Mamolos A.P., Kalburtji K.L., 2021. Could energy equilibrium and greenhouse gas emissions in agroecosystems play a key role in crop replacement? A case study in orange and kiwi orchards. *Environ. Sci. Pollut. Res*. 28, 29421–29431. DOI:10.1007/s11356-021-12774-4

Mostaghimi P., Kamali F., Jackson M.D., Muggeridge A.H., Pain C.C., 2016. Adaptive mesh optimization for simulation of immiscible viscous fingering. *SPE J*. 21, 6, 2250–2259.

Paidoussis M.P., 1998. *Fluid-Structure Interactions: Slender Structures and Axial Flow*. Academic Press, London.

Pałaszyńska K., Juszczak M., 2018. Gaseous emissions during agricultural biomass combustion in a 50 KW moving step grate boiler. *Chem. Proc. Eng.*, 39, 2, 197–208. DOI: 10.24425/119109.

Peters E., Broman J.A., Broman W.H., 1987. Computer image processing: a new tool for studying viscous fingering in corefloods. *SPE Reservoir Eng*. 2, 4, 720–728.

Pinilla A., Asuaje M., Ratkovich N., 2021. Experimental and computational advances on the study of Viscous Fingering: An umbrella review. *Heliyon* 7, 7, e07614. DOI:10.1016/j.heliyon.2021.e07614

Sinha S., Tarafdar S., 2009. Viscous fingering patterns and evolution of their fractal dimension. *Ind. Eng. Chem. Res*. 48, 19, 8837–8841.

Singh A., Singh Y., Pandey K.M., 2020. Viscous fingering instabilities in radial Hele-Shaw cell: A review. *Mater. Today: Proc*. 26. DOI:10.1016/j.matpr.2020.01.022

Wang M., Xiong Y., Liu L., Peng G., Zhang Z., 2019. Lattice Boltzmann simulation of immiscible displacement in porous media: viscous fingering in a shear-thinning fluid. *Trans. Por. Media*, 126, 2, 411–429.

Yang X., Tang Y., Li M., Li C., Wang M., Li X., Zhao J., 2022. Effect of shear-thinning of non-Newtonian fluid on the crossover from capillary fingering to viscous fingering in porous media. *Phys. Lett. A*, 449, 128364. DOI:10.1016/j.physleta.2022.128364

Yousefi M., Khoramivafa M., Damghani A.M., 2017. Water footprint and carbon footprint of the energy consumption in sunflower agroecosystems. *Environ. Sci. Pollut. Res*. 24, 19827–19834. DOI:10.1007/s11356-017-9582-4

Zhang C., Oostrom M., Grate J.W., Wietsma T.W., Warner M.G., 2011a. Liquid CO_2 displacement of water in a dual-permeability pore network micromodel. *Environ. Sci. Technol*. 45, 17, 7581–7588.

Zhang C., Oostrom M., Wietsma T.W., Grate J.W., Warner M.G., 2011b. Influence of viscous and capillary forces on immiscible fluid displacement: pore-scale experimental study in a water-wet micromodel demonstrating viscous and capillary fingering. *Energy Fuels*, 25, 8, 3493–3505. DOI:10.1021/ef101732k.